Journal of Power Sources 203 (2012) 227–232

Contents lists available at SciVerse ScienceDirect

Journal of Power Sources

journal homepage: www.elsevier.com/locate/jpowsour

Exfoliated graphite nanoplatelets–V_2O_5 nanotube composite electrodes for supercapacitors

Jeliza S. Bonso[a], Abdelaziz Rahy[a], Sanjaya D. Perera[a], Nijem Nour[b], Oliver Seitz[b], Yves J. Chabal[b], Kenneth J. Balkus Jr.[a,*], John P. Ferraris[a,*], Duck J. Yang[a,*]

[a] Department of Chemistry and the Alan G. MacDiarmid NanoTech Institute, The University of Texas at Dallas, 800 W. Campbell Road, Richardson, TX 75080, United States
[b] Department of Materials Science and Engineering, The University of Texas at Dallas, 800 W. Campbell Road, Richardson, TX 75080, United States

ARTICLE INFO

Article history:
Received 20 July 2011
Received in revised form
23 September 2011
Accepted 23 September 2011
Available online 1 October 2011

Keywords:
Electrochemical capacitors
Supercapacitors
Exfoliated graphite nanoplatelets
V_2O_5 nanotubes

ABSTRACT

Exfoliated graphite nanoplatelet (xGnP) and V_2O_5 nanotube (VNT) composite electrodes were fabricated and tested as electrodes for supercapacitors. Enhancement of the electrochemical performance of the composite over its component materials was demonstrated using cyclic voltammetry (CV), constant current charge/discharge testing and electrochemical impedance spectroscopy in aqueous and organic electrolytes. The calculated specific capacitance of the composite was 35 F g^{-1} in the aqueous electrolyte and 226 F g^{-1} in the organic electrolyte at a scan rate of 10 mV s^{-1} using a three-electrode system. Asymmetric coin cell devices were fabricated using activated carbon cloth as the positive electrode and xGnP–VNT composite as the negative electrode. The energy and power densities in 1 M LiTFSI were 28 Wh kg^{-1} and 303 W kg^{-1}, respectively, at a discharge current density of 250 mA g^{-1}.

Published by Elsevier B.V.

1. Introduction

Energy storage devices that possess both high energy and power densities with excellent cycling ability have been the subject of considerable interest [1]. Whereas batteries can provide high energy and capacitors can provide high power, supercapacitors exhibit intermediate energy and power densities [2,3]. Supercapacitors can be charged and discharged within seconds and have long cycling life ($\geq 10^5$ cycles) [4]. Also known as ultracapacitors or electrochemical capacitors (ECs), these devices store energy as charge on the electrode surface, rather than in the bulk material as in batteries. As a result, the electrode does not undergo drastic structural changes upon cycling [5]. ECs can be divided into two groups: electrochemical double layer capacitors (EDLCs) and pseudocapacitors. In EDLCs, the energy is stored electrostatically at the electrode–electrolyte interface in the double layer [6]. In contrast, in pseudocapacitors, charge storage occurs via fast redox reactions on the electrode surface [7].

Different carbon-based materials such as activated carbon, mesoporous carbon and carbon nanotubes have been used as electrodes in electrochemical double layer capacitors (EDLCs) [8,9]. Since the purely electrostatic mechanism of charge-storage depends on the surface area of the electrode material, EDLCs often exhibit low energy density values [8]. High surface area materials such as nanoporous carbide-derived carbon [10–13] and carbonized electrospun polymers [14,15] with improved energy and power densities have been reported. Pseudocapacitors involve redox active materials such as conducting polymers (polyaniline, polypyrrole and polythiophene) [3,16,17] or metal oxides such as (MnO_2, V_2O_5, and RuO_2) [18–20]. Pseudocapacitors exhibit much higher specific capacitance than EDLCs. For example, RuO_2 has a theoretical specific capacitance of 1340 F g^{-1} [20] but is expensive and like most metal oxides suffers from low conductivity [21]. Composite electrodes based on metal oxides and high surface area conductive carbon may combine the advantages of each material.

Graphene has been found to be suitable for energy storage applications because of its high specific surface area (2675 m^2 g^{-1}) and high electrical conductivity [22]. Graphene is a two-dimensional, one atom thick planar sheet of sp^2 bonded carbons. The use of graphene as electrodes for supercapacitors has been reported [23–25]. However, the generally observed specific capacitance of graphene is lower than expected due to restacking of the graphene sheets. To improve the capacitance performance, researchers have explored graphene-based composite materials. Wu et al. have reported a supercapacitor comprising graphene and polyaniline nanofibers that showed a capacitance of 210 F g^{-1} at a discharge rate of 0.3 A g^{-1} [26]. Other metal oxides such as MnO_2, ZnO and SnO_2 have been mixed with graphene to form composite electrodes with enhanced stability and energy density [27–29].

* Corresponding authors. Tel.: +1 972 883 2901; fax: +1 972 883 2925.
E-mail addresses: balkus@utdallas.edu (K.J. Balkus Jr.), ferraris@utdallas.edu (J.P. Ferraris), djyang@utdallas.edu (D.J. Yang).

0378-7753/$ – see front matter. Published by Elsevier B.V.
doi:10.1016/j.jpowsour.2011.09.084

In this work, a nanocomposite material composed of exfoliated graphite nanoplatelets (xGnP) and V_2O_5 nanotubes (VNT) was fabricated and tested as an electrode material for supercapacitors for the first time. Exfoliated graphite nanoplatelets are a few layers of graphene (<10 nm thick) that are produced from natural graphite without extensive chemical treatment [30]. Exfoliated graphite nanoplatelets have been reported to enhance the mechanical and electrical properties of polymers and metal oxides for different applications [31]. Vanadium pentoxide has been reported as supercapacitor electrode material owing to its high lithium intercalation capacity [32,33]. We report that the xGnP–VNT composite electrodes show increased electrochemical performance relative to the individual components.

2. Experimental

2.1. Materials

Exfoliated graphite nanoplatelets (xGnP) were obtained from XG Sciences (Grade M). Ammonium meta-vanadate (NH_4VO_3), DOWEX 50WX8-100 (100–200 mesh) and ethylene glycol (anhydrous, 99.8%) were purchased from Sigma–Aldrich. The electrolytes, KCl (>99%, Fisher Scientific) and lithium bis(trifluoromethanesulfonyl)imide (99.9%, 3 M), were used without further purification. Acetonitrile was obtained from Sigma–Aldrich and was dried (<15 ppm water content) using an MBraun Solvent Purification system prior to use. PVdF was purchased from Alfa-Aesar while Super P conducting additive was obtained from Timcal, Inc. Spectracarb 2225 (surface area = 2250 $m^2\,g^{-1}$) was obtained from Engineered Fibers Technology, LLC.

2.2. Preparation of exfoliated graphene nanoplatelets (xGnPs)

Commercially available exfoliated graphene nanoplatelets were dispersed in ethylene glycol by ultrasonication for 24 h. The dispersion was then filtered and dried at 100 °C for at least 12 h prior to use.

2.3. Synthesis of V_2O_5 nanotubes

The synthesis of V_2O_5 nanotubes was carried out using a sol–gel method [34]. V_2O_5 sol was prepared by mixing 0.8 g of ammonium meta-vanadate (NH_4VO_3) and 8 g of an acidic ion exchange resin (DOWEX 50WX8-100) in 160 ml DI water. The mixture was heated at 60 °C for 20 min to produce an orange colored sol. After cooling to room temperature, 50 ml of the V_2O_5 sol was mixed with 50 ml of ethanol and left at room temperature with no agitation for 7 days. The final greenish product was filtered, washed with DI water and ethanol and dried at 100 °C.

2.4. Preparation of xGnP–VNT composite

xGnP (0.3 g) was bath sonicated in 100 ml of ethanol for 1 h. Then a 50 ml portion of the prepared orange V_2O_5 sol was mixed with the xGnPs/ethanol dispersion and stirred for 7 days. The final product, xGnP–VNT composite, was filtered, washed with DI water and ethanol and dried at 100 °C.

2.5. Characterization

The xGnP–VNT composite was characterized by SEM, TEM, XRD, XPS and Raman spectroscopy. The morphology of each sample was determined by using a Zeiss Supra™ 40 variable-pressure field-effect scanning electron microscope. TEM samples were prepared on carbon coated copper grids and images were obtained using a JEOL 2100 transmission electron microscope at 200 kV. Raman spectra were collected using a JobinYvon HORIBA Raman spectrometer. XRD patterns were collected using a Rigaku Ultima IV X-ray diffractometer (Cu Kα). XPS analysis was done *ex situ* using a PerkinElmer PHI System with monochromatic Al Kα radiation ($h\nu$ = 1486.6 eV) detector with 45° emission angle (0.125 eV step size, pass energy of 29.35 eV) at 3×10^{-9} Torr chamber pressure.

2.6. Electrode fabrication and testing

A three-electrode system was employed to compare the electrochemical properties of the xGnPs, VNTs and xGnP–VNT composites. The electrodes were prepared by mixing the xGnP–VNT composite, Super P (10%) as conductive additive and PVdF (30%) as binder in acetone. The xGnP and VNT electrodes were also prepared using the same procedure. The xGnP–VNT slurry was coated onto 1 cm^2 graphite foil, which was used as the working electrode. The counter and reference electrodes were Pt mesh and Ag/Ag^+, respectively. Cyclic voltammetry was performed in aqueous (2 M KCl) and organic (1 M LiTFSI in acetonitrile) electrolytes using a Princeton Applied Research (PAR 273A) Galvanostat/Potentiostat.

Two-electrode coin cell devices were assembled using the xGnP–VNT composite as the negative electrode and an activated carbon cloth (Spectracarb 2225) as the positive electrode. The xGnP–VNT electrode was prepared from the slurry that was cast on a glass plate to form ~100 μm thick film. Circular electrodes (1 cm^2) were pressed together in a 2032 stainless steel coin cell using a manual crimper. A Gore™ PTFE film was used as the separator and was soaked in 1 M LiTFSI. All cells were equilibrated for 10 cycles at 10 mV s^{-1} prior to obtaining measurements. Cyclic voltammetry and charge discharge tests were used to calculate the electrochemical performance using an Arbin Supercapacitor Test Station. Electrochemical impedance spectroscopy was done using a PAR 2273 at 0 V DC from 100 kHz to 1 MHz with an AC voltage of 10 mV.

3. Results and discussion

Fig. 1A and B shows SEM images of the xGnPs before and after loading with VNTs. The VNTs appear to cover most of the xGnP sheets (Fig. 1B). This arrangement is favorable because the possible restacking of the nanoplatelets can be prevented by the VNTs that coat the xGnP surface. Fig. 1C and D shows the fabricated electrode which is ~100 μm thick. TEM images (Fig. 2A) show the nanotubular structure of V_2O_5 with an outer diameter of ~10 nm and an inner diameter of ~5 nm. These V_2O_5 nanotubes are among the smallest diameter nanotubes reported [35–40]. Higher magnification revealed the interlayer distance of the VNTs to be about 0.5 nm. The TEM image of the composite (Fig. 2B) shows a sub-micron to micron lateral dimension of the exfoliated graphite sheets and no significant changes in V_2O_5 nanotube morphology.

The Raman spectrum of xGnP (Fig. 3a) shows the G peak at 1575 cm^{-1}, which is characteristic of sp^2 carbon vibration in the graphitic lattice. A smaller D-peak is also observed at 1329 cm^{-1}, which is mainly due to the disordered or amorphous carbon [41]. A Raman feature called the G′ peak corresponding to second order vibration of sp^2 exfoliated graphite sheets appears at 2675 cm^{-1} [42]. From its peak position and intensity relative to the G peak, the xGnP has >10 layers of graphene sheets. The Raman spectra of crystalline V_2O_5 is also shown (Fig. 3b). The tallest peak, at 143 cm^{-1}, can be assigned to the skeleton vibration of the V–O–V bond, which can be assigned to the deformation of the bond between different molecular units in the plane of the layers. The peak at 991 cm^{-1} is due to the stretching mode of the double bond between vanadium and oxygen atoms (V=O) [43]. The peaks 692 cm^{-1} and 524 cm^{-1}

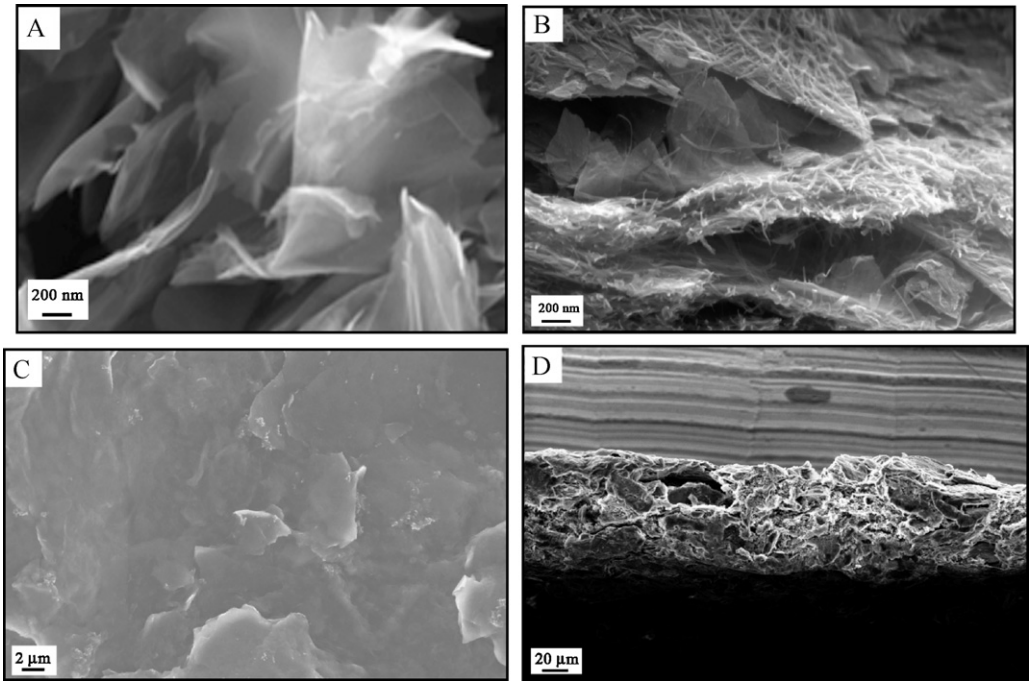

Fig. 1. SEM images of (A) xGnP, (B) xGnP–VNT, (C) top and (D) cross-section view of the composite electrode with binder.

are also observed and correspond to V_2–O (doubly coordinated oxygen) and V_3–O (triply coordinated oxygen), respectively [44]. The bending modes in V_2O_5 are also observed at 405 cm^{-1} and 283 cm^{-1} for V=O, 478 cm^{-1} for (V_3–O) and 303 cm^{-1} (V_3–O) [45]. The Raman spectrum of the composite (Fig. 3c) shows the characteristic peaks from the individual components.

The XRD pattern (Fig. 4) of the VNTs shows its tallest peak at $2\theta = 7.52$, corresponding to the (0 0 1) diffraction plane of hydrous V_2O_5 [46]. The d-spacing using the Bragg equation ($n\lambda = 2d \sin\theta$) is 1.17 nm. The peaks at $2\theta = 23$, 31, 40 and 51° could be assigned to the (0 0 2), (0 0 3) and (0 0 4) diffraction, respectively. From the TEM image (Fig. 2A), the inter-tube distance corresponds to the (0 0 3) diffraction, which is about 0.4 nm. The X-ray photoelectron spectroscopy (XPS) analysis of the V_2O_5 nanotubes shows a peak at 517.25 eV, which is due to the main binding energy of the V $2p^{3/2}$ electrons (Fig. 5). The deconvoluted spectrum shows a peak at 516 eV due to the partial reduction from +5 oxidation state to +4 of vanadium. Based on the peak areas, the vanadium +4/+5 ratio is ~0.09.

Table 1
Summary of C_{sp} values of xGnP, VNT and the composite in aqueous and organic electrolytes.

Electrode	Specific capacitance (F g^{-1}) at 10 mV s^{-1}	
	In 2 M KCl	In 1 M LiTFSI
xGnP	15 ± 0.5	42.5 ± 0.5
VNT	25.5 ± 2.5	70 ± 3
xGnP–VNT	35 ± 1	226 ± 14

Higher specific capacitance values were obtained for the composite electrode compared to individual component electrodes for both aqueous and organic electrolytes (Table 1). In 2 M KCl, the CV plot displayed a rectangular shape characteristic of an ideal capacitor. Fig. 6 shows the CV plot of the composite measured in 2 M KCl

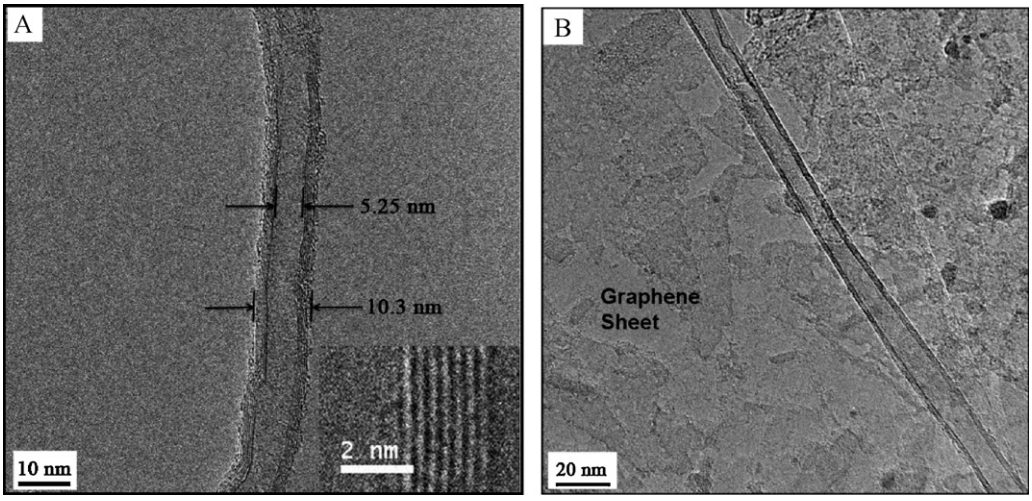

Fig. 2. TEM images of (A) VNTs and (B) xGnP–VNT composite.

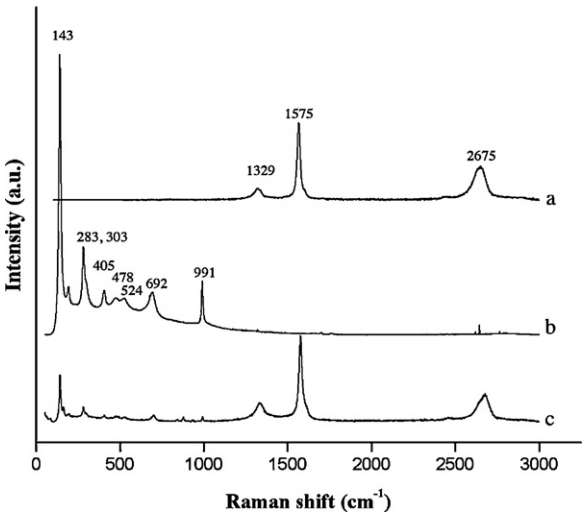

Fig. 3. Raman spectra of (a) xGnP, (b) VNT and (c) xGnP–VNT.

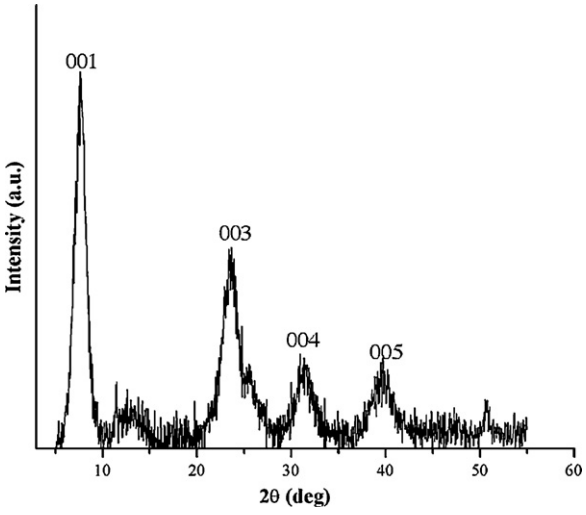

Fig. 4. XRD pattern of VNTs.

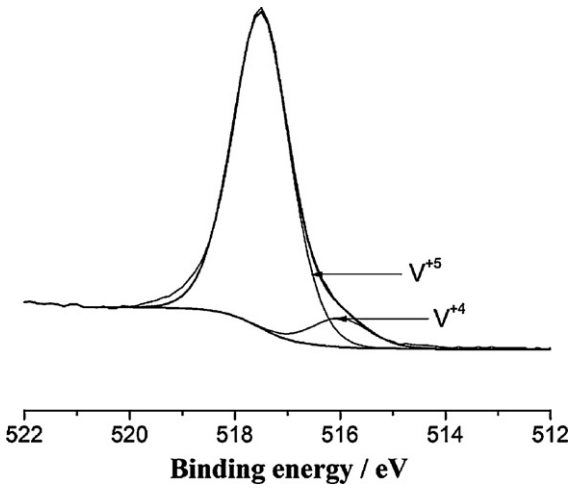

Fig. 5. XPS spectra of xGnP–VNT composite.

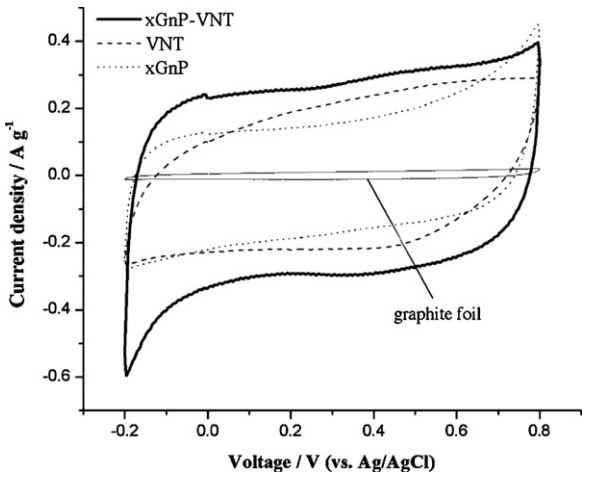

Fig. 6. Cyclic voltammograms of xGnP, VNT and the composite in 2 M KCl at 10 mV s^{-1}.

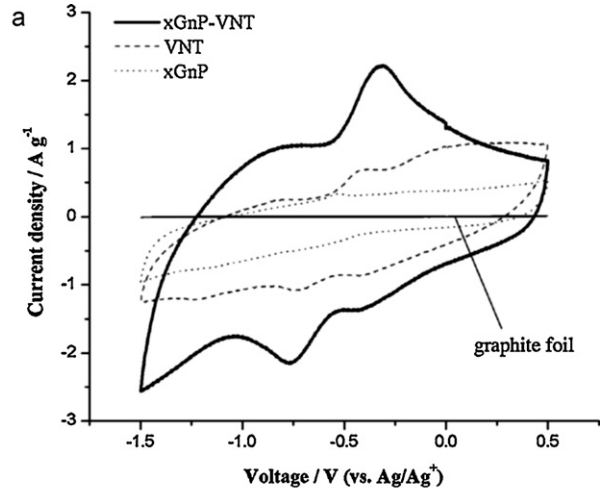

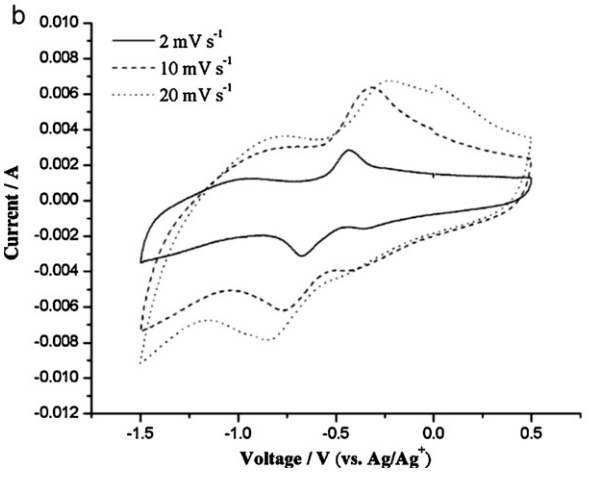

Fig. 7. (A) CV plots of xGnP, VNT and the xGnP–VNT in 1 M LiTFSI at 10 mV s^{-1}. (B) CV of xGnP–VNT in 1 M LiTFSI at different scan rates.

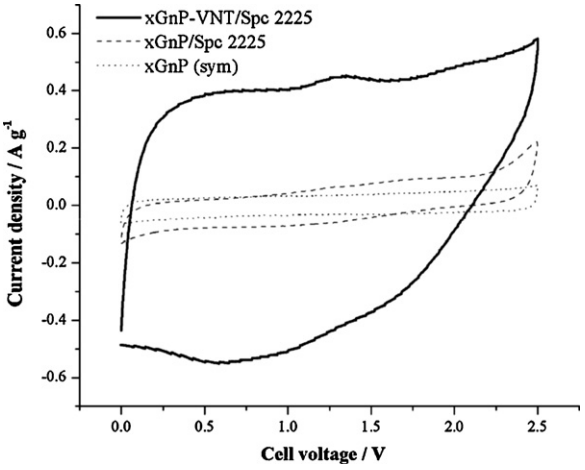

Fig. 8. Cyclic voltammogram at 10 mV s^{-1} in 1 M LiTFSI in acetonitrile of asymmetric xGnP–VNT/Spectracarb carbon cloth device.

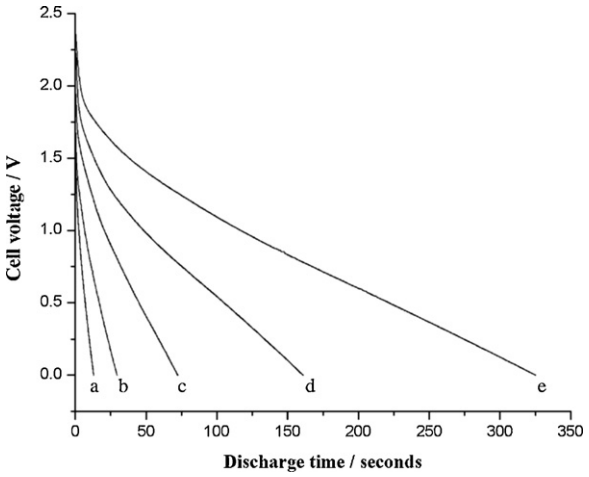

Fig. 9. Cell voltage vs. discharge time of Spectracarb 2225/xGnP–VNT asymmetric supercapacitor in 1 M LiTFSI. Discharge current densities (a–e) correspond to 4, 2, 1, 0.5 and 0.25 A g^{-1}, respectively.

(pH 2.45) at scan rate of 10 mV s^{-1}, which gave a specific capacitance of 35 F g^{-1}. The specific capacitance (C_{sp}) is calculated from the area under the discharge curve of the cyclic voltammogram using the formula:

$$C_{sp} = \int \frac{it}{Vm} dt$$

where *it* is the product of current (i) and time (t) along the voltage range (V) and (m) is the mass of the electrode.

V_2O_5 has been reported to have high lithium ion capacity with a theoretical value of 147 mAh g^{-1} as an anode [47]. The CV plot (Fig. 7) of the composite in 1 M LiTFSI shows peaks at 0.25 V in the anodic scan and at −0.38 V and −0.75 V in the cathodic scan, which can be attributed to the lithium intercalation/deintercalation process. The electrochemical Li insertion process that occurs at V_2O_5 electrodes can be expressed by $V_2O_5 + xLi^+ + xe^- \leftrightarrow Li_xV_2O_5$ [48]. The specific capacitance obtained for the composite in 1 M LiTFSI in acetonitrile was 226 F g^{-1}, which is higher compared to xGnPs or VNTs (Table 1). The result obtained for xGnPs is comparable to previously reported value of multi-layered xGnP sheets with different sizes [49].

An asymmetric device was constructed in which the xGnP–VNT composite served as the negative electrode and a Spectracarb 2225 activated carbon cloth was used as the positive electrode. The measured specific capacitance of a symmetric carbon cloth device in 1 M LiTFSI based only on the mass of the electrodes was 28 F g^{-1}. The asymmetric device shows a rectangular CV (Fig. 8) with a specific capacitance of 42 F g^{-1} at 10 mV s^{-1}. Constant-current charge–discharge tests in 1 M LiTFSI in acetonitrile were collected at a rated voltage of 2.5 V. The discharge profile of the asymmetric cell (Spectracarb 2225/xGnP–VNT) at different discharge current densities is shown in Fig. 9. The initial coulombic efficiency of the device was 91.5% (Fig. 10A). After 300 cycles, there was a 22% decrease in C_{sp} while the coulombic efficiency was maintained at 98% (Fig. 10B). The Ragone plot shown in Fig. 11 indicates the highest energy density obtained for Spectracarb 2225/xGnP–VNT was 28 Wh kg^{-1} with power density of 303 W kg^{-1} at 250 mA g^{-1} discharge current based only on the active electrode mass. Even at a higher discharge density of 5 A g^{-1}, the asymmetric device provides 10 Wh kg^{-1} at 4 kW kg^{-1}, which implies that the composite can be used for applications requiring both high energy and power densities.

In the Nyquist plot (Fig. 12), a semi-circle is observed in the high-frequency region and is related to the electrolyte resistance. From the *x*-intercept of the Nyquist plot, an equivalent series resistance (ESR) of 1.78 Ω is obtained. This value is related to power density by the equation $P = V^2/4ESR$. Over the frequency range of 400 Hz to 2 Hz, another semi-circular feature is observed, which may be attributed to the lithium intercalation process as observed in V_2O_5 nanowire and Li_xCoO_2 electrodes [32,50]. A nearly vertical line is observed in the low-frequency region, which is indicative of ideal capacitive behavior. The results show that the xGnP–VNT composite is a suitable negative electrode for supercapacitors.

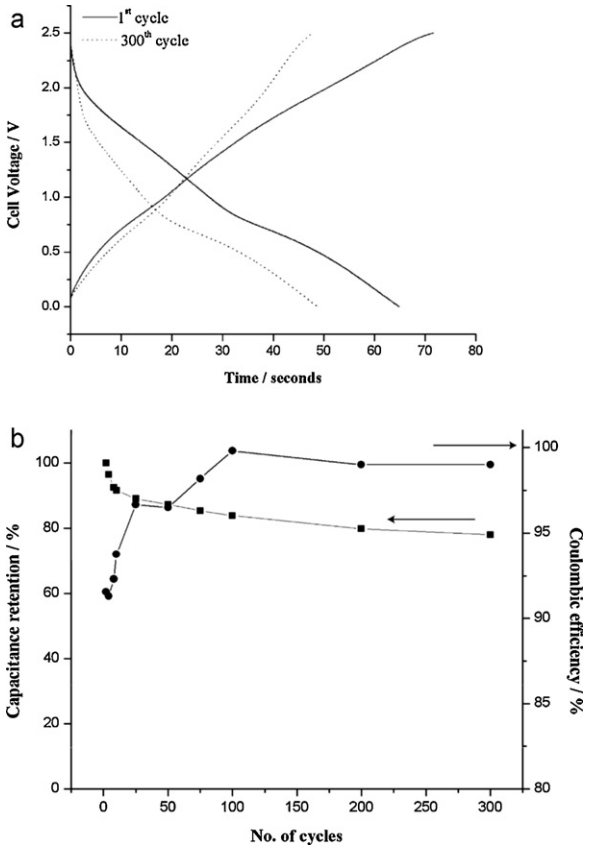

Fig. 10. (A) Charge–discharge profile of Spectracarb 2225/xGnP–VNT asymmetric supercapacitor in 1 M LiTFSI at 1 A g^{-1} for the 1st and 300th cycle. (B) Capacitance retention and coulombic efficiency of Spectracarb 2225/xGnP–VNT asymmetric supercapacitor for 300 cycles.

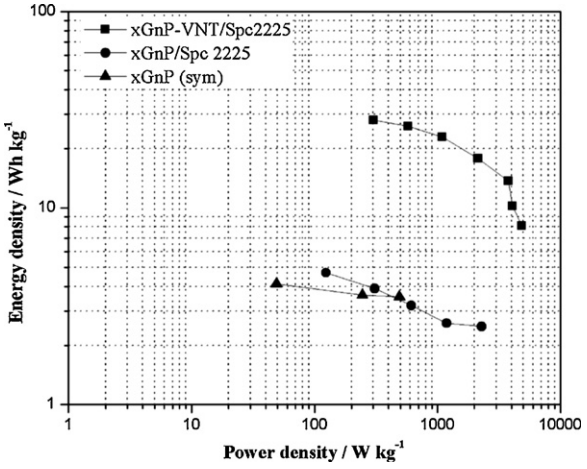

Fig. 11. Ragone plot of the Spectracarb 2225/xGnP–VNT asymmetric device.

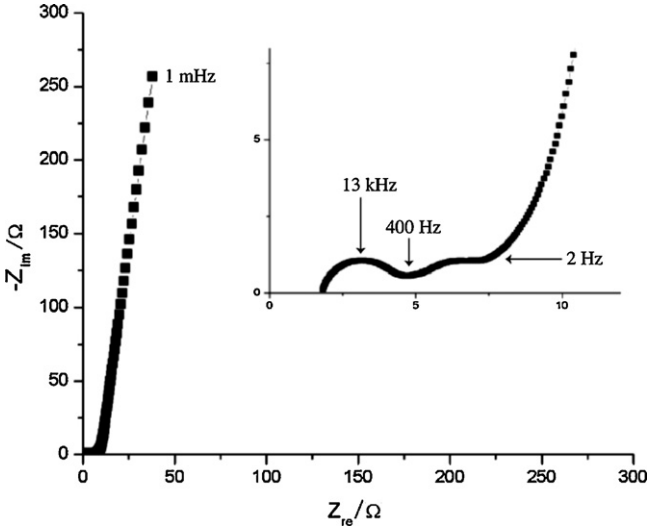

Fig. 12. Nyquist plot of Spectracarb 2225/xGnP–VNT composite from 100 kHz to 1 MHz.

4. Conclusion

The xGnP–VNT composite exhibited improved electrochemical performance of electrodes for supercapacitors over its components. Specific capacitance value of 226 F g^{-1} was measured in 1 M LiTFSI in acetonitrile for the xGnP–VNT composite. In contrast, the specific capacitance of just VNTs was 70 F g^{-1} and just xGnP was 42.5 F g^{-1}, demonstrating the synergistic effect of combining the two materials. An asymmetric device using Spectracarb 2225 carbon cloth as the counter electrode produced an energy density of 28 Wh kg^{-1} and 303 W kg^{-1} at 100 mA g^{-1} and 10 Wh kg^{-1} and 4075 W kg^{-1} at a higher discharge current of 5 A g^{-1}.

Acknowledgements

The authors gratefully acknowledge DOE grant (DE-EE0004156) and AFRL grant (R15906) for funding. A partial support from University of Dayton Research Institute/Korea Electronic Technology Institute is also appreciated.

References

[1] A. Burke, J. Power Sources 91 (2000) 37–50.
[2] M. Winter, R.J. Brodd, Chem. Rev. 104 (2004) 4245–4270.
[3] G.A. Snook, P. Kao, A.S. Best, J. Power Sources 196 (2011) 1–12.
[4] A. Du Pasquier, I. Plitz, S. Menocal, G. Amatucci, J. Power Sources 115 (2003) 171–178.
[5] M.S. Whittingham, MRS Bull. 33 (2008) 411–419.
[6] R. Kotz, M. Carlen, Electrochim. Acta 45 (2000) 2483–2498.
[7] B.E. Conway, V. Birss, J. Wojtowicz, J. Power Sources 66 (1997) 1–14.
[8] L.L. Zhang, X.S. Zhao, Chem. Soc. Rev. 38 (2009) 2520–2531.
[9] S.M.I. Riccardo Signorelli, D.C. Ku, J.G. Kassakian, J.E. Schindall, Proc. IEEE 97 (2009) 1837–1847.
[10] M. Arulepp, J. Leis, M. Lätt, F. Miller, K. Rumma, E. Lust, A.F. Burke, J. Power Sources 162 (2006) 1460–1466.
[11] T. Thomberg, A. Jänes, E. Lust, J. Electroanal. Chem. 630 (2009) 55–62.
[12] H. Kurig, A. Janes, E. Lust, J. Electrochem. Soc. 157 (2010) A272.
[13] M. Heon, S. Lofland, J. Applegate, R. Nolte, E. Cortes, J.D. Hettinger, P.-L. Taberna, P. Simon, P. Huang, M. Brunet, Y. Gogotsi, Energy Environ. Sci. 4 (2011) 135.
[14] N.-N. Bui, B.-H. Kim, K.S. Yang, C.M.E. Dela, J.P. Ferraris, Carbon (NY) 47 (2009) 2538–2539.
[15] S.K. Nataraj, B.H. Kim, C.M. dela, J. Ferraris, T.M. Aminabhavi, K.S. Yang, Mater. Lett. 63 (2009) 218–220.
[16] A. Rudge, I. Raistrick, S. Gottesfeld, J.P. Ferraris, Electrochim. Acta 39 (1994) 273–287.
[17] J.P. Ferraris, M.M. Eissa, I.D. Brotherston, D.C. Loveday, Chem. Mater. 10 (1998) 3528–3535.
[18] M. Toupin, T. Brousse, D. Belanger, Chem. Mater. 14 (2002) 3946–3952.
[19] G. Wee, H.Z. Soh, Y.L. Cheah, S.G. Mhaisalkar, M. Srinivasan, J. Mater. Chem. 20 (2010) 6720–6725.
[20] C.-C. Hu, W.-C. Chen, K.-H. Chang, J. Electrochem. Soc. 151 (2004) A281–A290.
[21] O. Barbieri, M. Hahn, A. Foelske, R. Kotz, J. Electrochem. Soc. 153 (2006) A2049.
[22] C. Liu, Z. Yu, D. Neff, A. Zhamu, B.Z. Jang, Nano Lett. 10 (2010) 4863–4868.
[23] D.A.C. Brownson, D.K. Kampouris, C.E. Banks, J. Power Sources 196 (2011) 4873–4885.
[24] S. Vivekchand, C. Rout, K. Subrahmanyam, A. Govindaraj, C. Rao, J. Chem. Sci. 120 (2008) 9–13.
[25] M.D. Stoller, S.J. Park, Y.W. Zhu, J.H. An, R.S. Ruoff, Nano Lett. 8 (2008) 3498–3502.
[26] Q. Wu, Y.X. Xu, Z.Y. Yao, A.R. Liu, G.Q. Shi, ACS Nano 4 (2010) 1963–1970.
[27] Z.-S. Wu, W. Ren, D.-W. Wang, F. Li, B. Liu, H.-M. Cheng, ACS Nano 4 (2010) 5835–5842.
[28] T. Lu, Y. Zhang, H. Li, L. Pan, Y. Li, Z. Sun, Electrochim. Acta 55 (2010) 4170–4173.
[29] F. Li, J. Song, H. Yang, S. Gan, Q. Zhang, D. Han, A. Ivaska, L. Niu, Nanotechnology 20 (2009) 455602.
[30] K. Kalaitzidou, H. Fukushima, P. Askeland, L.T. Drzal, J. Mater. Sci. 43 (2008) 2895–2907.
[31] K. Kalaitzidou, H. Fukushima, L.T. Drzal, Carbon (NY) 45 (2007) 1446–1452.
[32] S.D. Perera, B. Patel, N. Nijem, K. Roodenko, O. Seitz, J.P. Ferraris, Y.J. Chabal, K.J. Balkus, Adv. Energy Mater. 1 (2011) 936–945.
[33] S.-I. Pyun, J.-S. Bae, J. Power Sources 68 (1997) 669–673.
[34] G. Gu, M. Schmid, P.-W. Chiu, A. Minett, J. Fraysse, G.-T. Kim, S. Roth, M. Kozlov, E. Muñoz, R.H. Baughman, Nat. Mater. 2 (2003) 316–319.
[35] Y. Wang, G. Cao, Chem. Mater. 18 (2006) 2787–2804.
[36] J. Emmerich, M. Dillen, C.E.A. Kirschhock, J.A. Martens, Stud. Surf. Sci. Catal. 175 (2010) 249–252.
[37] V.M. Mohan, B. Hu, W. Qiu, W. Chen, J. Appl. Electrochem. 39 (2009) 2001–2006.
[38] C. O'Dwyer, V. Lavayen, D.A. Tanner, S.B. Newcomb, E. Benavente, G. Gonzalez, T.C.M. Sotomayor, Adv. Funct. Mater. 19 (2009) 1736–1745.
[39] V.L. Volkov, G.S. Zakharova, Russ. J. Inorg. Chem. 54 (2009) 36–39.
[40] A. Gloskovskii, S.A. Nepijko, G. Schonhense, H.A. Therese, A. Reiber, H.C. Kandpal, G.H. Fecher, C. Felser, W. Tremel, M. Klimenkov, J. Appl. Phys. 101 (2007), 084301/1–084301/6.
[41] M.S. Dresselhaus, A. Jorio, M. Hofmann, G. Dresselhaus, R. Saito, Nano Lett. 10 (2010) 751–758.
[42] L.M. Malard, M.A. Pimenta, G. Dresselhaus, M.S. Dresselhaus, Phys. Rep. 473 (2009) 51–87.
[43] C. Sanchez, J. Livage, G. Lucazeau, J. Raman Spectrosc. 12 (1982) 68–72.
[44] B. Yan, L. Liao, Y. You, X. Xu, Z. Zheng, Z. Shen, J. Ma, L. Tong, T. Yu, Adv. Mater. (Weinheim, Germany) 21 (2009) 2436–2440.
[45] S.-H. Lee, H.M. Cheong, M.J. Seong, P. Liu, C.E. Tracy, A. Mascarenhas, J.R. Pitts, S.K. Deb, Solid State Ionics 165 (2003) 111–116.
[46] W. Avansi Jr., C. Ribeiro, E.R. Leite, V.R. Mastelaro, J. Cryst. Growth 312 (2010) 3555–3559.
[47] E.A. Olivetti, K.C. Avery, I. Taniguchi, D.R. Sadoway, A.M. Mayes, J. Electrochem. Soc. 155 (2008) A488–A493.
[48] Z. Chen, V. Augustyn, J. Wen, Y. Zhang, M. Shen, B. Dunn, Y. Lu, Adv. Mater. 23 (2011) 791–795.
[49] S. Biswas, L.T. Drzal, ACS Appl. Mater. Interfaces 2 (2010) 2293–2300.
[50] J. Zhao, L. Wang, X. He, C. Wan, C. Jiang, Int. J. Electrochem. Sci. 5 (2010) 478–488.